Tang, J., Swolfs, Y., Longana, M., Yu, H., Wisnom, M., Lomov, S. V., & Gorbatikh, L. (2019). Hybrid composites of aligned discontinuous carbon fibers and self-reinforced polypropylene under tensile loading. *Composites Part A: Applied Science and Manufacturing*, *123*, 97-107. https://doi.org/10.1016/j.compositesa.2019.05.003

# Hybrid composites of aligned discontinuous carbon fibers and self-reinforced polypropylene under tensile loading

Jun Tang[1*], Yentl Swolfs[1], Marco L. Longana[2], HaNa Yu[2,3], Michael R. Wisnom[2], Stepan V. Lomov[1], Larissa Gorbatikh[1]

[1]Department of Materials Engineering, KU Leuven, Kasteelpark Arenberg 44 box 2450, 3001 Leuven, Belgium

[2]Bristol Composites Institute (ACCIS), University of Bristol, BS8 1TR, Bristol, UK

[3]Department of Mechanical Engineering, University of Bath, BA2 7AY, Bath, UK

**Abstract:** Highly aligned discontinuous fiber composites have demonstrated mechanical properties comparable to those of unidirectional continuous fiber composites. However, their ductility is still limited by the intrinsic brittleness of the fibers and stress concentrations at the fiber ends. Hybridization of aligned discontinuous carbon fibers (ADCF) with self-reinforced polypropylene (SRPP) is a promising strategy to achieve a balanced performance in terms of stiffness, provided by the ADCF, and ductility, delivered by SRPP. The current work focuses on interlayer hybridization of these materials and their tensile behavior as a function of different material parameters. Effects of the carbon layer thickness, carbon/SRPP layer thickness ratio, layer dispersion and interface adhesion are investigated. The carbon fiber misalignment is characterized using X-ray computed tomography to predict the modulus of the aligned discontinuous carbon fiber layer. The hybrids exhibit a gradual tensile failure with high pseudo-ductile strain of above 10% facilitated by multiple carbon layer failures (layer fragmentation) and dispersed delaminations. At the microscopic scale, the carbon layer fails mainly through interfacial debonding and fiber pull-out.

**Keywords:** A. Discontinuous reinforcement; A. Hybrid; B. Fragmentation; B. Delamination

## 1. Introduction

Discontinuous fiber-reinforced composites have been widely applied in the automotive industry due to their cost-efficiency, superior formability, and good mechanical properties [1]. Several numerical studies [2-4] have demonstrated that discontinuous fiber-reinforced composites can achieve a balanced multi-property mechanical performance (stiffness, strength and toughness) by the following strategies:

(1) optimizing the fiber length [2]: the critical fiber length is the key factor governing the tensile strength of the short fiber composites as well as the transition from fiber end debonding to fiber breakage as the dominating damage mechanism;

(2) optimizing fiber orientation [4]: large orientation angles deviating from the loading direction lead to higher failure strain but lower stiffness and strength of the discontinuous carbon fiber/polypropylene (PP) composites; and

(3) optimizing fiber arrangement [3]: staggering fibers with a fixed overlap length (stair-wise) results in a better combination of stiffness, strength and toughness for unidirectional discontinuous fiber composites than for staggered fibers with random overlap lengths.

Aligning discontinuous fibers in the loading direction is crucial for optimizing the mechanical properties of the discontinuous fiber composites, but most of the studies rely on modeling work due to the difficulties in producing such composites. To align the short fibers in a preferential direction, several techniques, such as pneumatic [5] and flow-induced methods [6,7], have been developed in the past. Most recently, a novel manufacturing method for aligned discontinuous fiber composites, termed High Performance-Discontinuous Fiber (HiPerDiF) method, was invented [8]. This new method fabricates highly aligned discontinuous preforms directly from discontinuous fibers by suspending the discontinuous fibers in water and spraying the fiber suspension between several parallel plates. This technique is suited for production of polymer composites from recycled fibers [9-12], and is also applicable for mixing different fiber types [13] as well as fiber lengths [14].

However, aligned discontinuous fiber composites themselves could not reach sufficiently high failure strain. In most cases, the failure strain of aligned discontinuous fiber composites is lower than the failure strain of the fibers, as the discontinuities could lead to fiber-matrix debonding and act as stress concentrators. For instance, the ultimate failure strain is lower than 1.2% for aligned discontinuous carbon fiber-reinforced epoxy and lower than 1.0% for aligned discontinuous carbon fiber-reinforced PP [15], though both composites demonstrate a non-linear tensile behavior.

Hybridizing brittle fibers with more ductile fibers is a promising way to increase the ductility. The advantages of fiber-hybridization have been elaborated in the recent reviews by Swolfs et al. [16,17]. Though fiber-hybrid composites have been extensively investigated, most studies focused on continuous fibers, seldom on discontinuous fibers and even less on aligned discontinuous fibers. This creates a gap in understanding of how discontinuous fibers behave in the fiber-hybrids, and how the fiber-hybridization influences the mechanical properties of aligned discontinuous fiber composites.

The discontinuous fibers can be hybridized with discontinuous fibers as well as continuous fibers. Intermingled (fiber-by-fiber) aligned discontinuous carbon/glass fiber hybrids show an increase in ultimate failure strain with a decrease in carbon/glass ratio [13,18]. Finley et al [19] investigated the effect of fiber arrangements on the mechanical properties of aligned intermingled carbon/glass hybrid composites. A 44% increase in pseudo-ductile strain was predicted when the carbon fibers are completely isolated from one-another. Furthermore, Yu et al [20] manufactured a hierarchical hybrid composite by combining aligned discontinuous fibers and continuous fibers in a layer-by-layer manner. The resultant hybrid composite exhibits a much higher ultimate failure strain than that of aligned discontinuous fiber composites. Compared to continuous fiber-hybrids, the introduction of discontinuities in fiber-hybrids offers the opportunity to engineer a more gradual deformation and failure process by triggering micro-scale damage, including short fiber breakage or pull-out [20].

To date, the available research on hybridization of aligned discontinuous fibers with continuous fibers is mainly limited to classical fiber combinations such as carbon and glass. The ultimate failure strain of these aligned discontinuous fiber hybrid composites is still low (within few percents at most). In this study, we develop a novel hybrid composite by combining aligned discontinuous carbon fibers with highly ductile self-reinforced polypropylene (SRPP) with a failure strain of 20%. In our previous studies [21,22], the continuous carbon fiber/SRPP hybrids were often found to suffer from the sudden loss of load carrying capacity, which was due to the fracture of the carbon layer. By applying aligned discontinuous carbon fibers, it is expected to eliminate the sudden loss of load carrying capacity by promoting more gradual carbon layer

failure. The good alignment of the discontinuous carbon fibers also gives a reasonably high stiffness. The overall aim is to achieve a balanced performance in terms of stiffness and ductility. Understanding how this performance can be optimized through the laminate design and which failure mechanisms are responsible for producing a gradual (pseudo-ductile) failure is also of interest.

## 2. Materials and methods

### 2.1. Materials

The raw materials used in the study are PP tape fabric, homo-PP film, maleic-anhydride modified PP (MAPP) film and aligned discontinuous carbon fiber (ADCF) preforms.

The PP tape fabric and aligned discontinuous carbon fiber preform are shown in Fig. 1. The PP fabric with a twill 2/2 weave pattern was supplied by Propex Fabrics GmbH (Gronau, Germany). The areal density of the PP fabric was 130 g/m$^2$ and the density of the used PP grade was 0.92 g/cm$^3$. The compacted thickness of the PP fabric was calculated to be 141 µm. Propex Fabrics GmbH also provided PP and MAPP films. Both films had thickness of 20 µm. The PP film had the same PP grade as in the PP tape fabric. Due to the lack of active groups that can react with the functional groups on the carbon fiber surface, PP adheres poorly to carbon fibers [23]. With MAPP, the interfacial adhesion can be significantly enhanced compared to carbon fiber/PP [24,25]. This is attributed to the functional groups of maleic anhydride creating chemical bonding at the fiber/matrix interface.

The ADCF preform was manufactured by the HiPerDiF method at the University of Bristol [8]. The discontinuous carbon fiber used in the study was TENAX C124 with a length of 3 mm and its density was 1.82 g/cm$^3$ [8]. The produced ADCF preform had a width of 5 mm. The engineering constants of the raw materials are listed in Table 1 [8,22]. The ADCF preform had an areal density of around 70 g/m$^2$, which resulted in a compacted thickness of around 40 µm.

### 2.2. Composites manufacturing

Different hybrid composites were manufactured as listed in Table 2. The meaning of the notation of the layup is as follows: S stands for SRPP layer, $C^{PP}$ for CF/PP layer and $C^{MAPP}$ for CF/MAPP layer. The subscripts designate the number of layers. The manufacturing process can

be separated into two steps: 1) impregnation of ADCF preforms and 2) hot compaction of PP fabrics together with the produced prepregs. Four matrix films were added to the ADCF preform to impregnate the fibers: two on top and two below. The matrix films were either PP or MAPP depending on the designed hybrid layups in Table 2. The stack was hot pressed at 188 ºC and 5 bar for 5 min. Then, the resulting ADCF prepregs were placed closely next to each other to make a wide enough panel, so that specimens wider than 5 mm could be cut. To avoid the movement of the ADCF prepregs during the layup, the strip ends were taped onto the mold. The parallel arranged ADCF/PP strips and PP tape fabrics were then laid up with desired configurations. The stack was hot compacted at 188 ºC and 39 bar for 5 min. During the hot compaction, the outer sheath of the PP tapes was molten to form 'matrix', while leaving the un-molten core as the 'reinforcement'. A higher pressure compared to that used for impregnating the ADCF preform was applied in this case to prevent shrinkage of the PP tapes. These processing parameters have been carefully optimized, as described in [26]. This means that the void content in the resultant hybrid composite is low. The low void content in the ADCF layer in the hybrid composite can be proven by the X-ray computed tomographic image of a representative slice of the carbon fiber layer, see Fig. 2b. Moreover, the effect of voids is less severe in ductile materials than in brittle materials [27]. Therefore, the effect of void content is not considered in the current study, as SRPP is a ductile material.

**2.3. Tensile test**

The tensile behavior was characterized following the ASTM D3039 standard. The specimens were nominally 200 mm long and 10 mm wide and they were tested at the displacement rate of 5 mm/min with a gauge length of 100 mm (5% strain per min). Sandpaper was added in the gripping region to avoid slippage during the test. Due to the experimental nature of the material and its limited availability, only three specimens were tested per hybrid configuration. 2D digital image correlation (DIC) was applied to measure the strain on the speckled specimen surface.

The modulus was calculated as the slope between 0.1% and 0.3% strain. The strength is defined as the maximum stress reached. The ultimate failure strain is defined as the strain when SRPP layers fracture. In some cases, there are still few PP tapes left intact when SRPP layers

fracture. The elongation of these PP tapes is not included in the ultimate failure strain calculation. The carbon fiber layer failure leads to a significant drop in the overall sample stiffness, which causes the stress-strain curve to deviate from the initial linearity and is displayed as a sudden stress drop or a knee point. Therefore, the stress and strain at carbon layer failure are obtained from the peak point on the stress-strain diagram when there is a sudden stress drop. In the case of a knee point, the carbon layer failure point is defined as the intersection with a 0.2% strain offset.

### 2.4. Matrix burn-off test

To measure the overall carbon fiber volume fraction, $V_{f,h}$, in the hybrid composites, matrix burn-off tests were carried out according to the standard ASTM D2584. The specimens were heated in a porcelain crucible for a few minutes until the white smoke from the PP matrix ignition disappeared. Then, the specimens were put into a muffle furnace for 4 hours at 450 °C to remove the carbonaceous residue [28]. Weights of the specimens before and after matrix burn-off were measured on an electronic balance with an accuracy of 0.1 mg. The carbon fiber volume fraction was calculated based on the weight measurements and the densities of short carbon fiber (1.82 g/cm$^3$) and PP matrix (0.92 g/cm$^3$).

### 2.5. X-ray computed tomography

X-ray computed tomography (CT) was used to analyze the fiber orientation distribution [29–32] in the hybrid ADCF/SRPP composites. During the image acquisition the specimens were carefully centered on a sample holder and scanned with a Phoenix Nanotom system. A molybdenum target was used, and the scans were performed with a tube voltage of 60 kV and a current of 240 µA. The acquired tomographic images had a dimension of 2304 × 2304 pixels with a resolution of around 1.5 µm/pixel. After image acquisition, the micro-CT images were processed using the VoxTex software [33] developed at KU Leuven. This software converts the original micro-CT images into a three-dimensional array of 8-bit grey values. The fiber orientation can then be defined by a pair of angles, $\varphi$ and $\theta$, in a spherical coordinate system and the angles can be calculated based on the local structure tensor of the grey scale distribution. The values of the structure tensor and hence the orientation angles were determined on a voxel grid of $10^3$ pixels. The reader is referred to [32,33] for details of the orientation analysis.

## 3. Results and discussion

### 3.1. Fiber orientation distribution analysis

The fiber alignment is crucial for the stiffness and overall behavior of discontinuous fiber composites. The fiber orientation distribution analysis based on micro-CT data could be used for modulus prediction and sheds light on carbon layer failure mechanisms in Section 3.2.1.

Fig. 2a shows a representative cut-out volume of the hybrid specimen, and Fig. 2b demonstrates a horizontal slice of it, taken in the mid-plane of the ADCF/PP layer. Visual examination of Fig. 2b indicates that the discontinuous carbon fibers have a preferential orientation in the Z-direction, but their misalignment is evident. Analysis of the fiber orientation distribution in this section will quantify this misalignment. The definition of spatial and in-plane orientation angles is illustrated in Fig. 2c and d. The spatial orientation angle, $\theta_{XY}$, represents the overall deviation of the fiber from the Z direction, while the in-plane orientation angle, $\varphi_{ZX}$, is the deviation of the projected fiber onto the ZX plane from the Z direction.

Three specimens per hybrid layup were cut from different locations in the specimen and were scanned to have more representative results. The cumulative orientation angle distributions (both in-plane and spatial orientation angle) are plotted in Fig. 3a and b. As can be seen from Fig. 3a, the fibers are preferentially aligned in the 0º direction (coinciding with Z direction). 67% of the fibers in the hybrids are within ±10º and around 30% fibers are within ±3º, see Fig. 3c. Comparing the percentage of fibers within ±3º in the current study to that reported in the literature for composites with discontinuous carbon fibers from the HiPerDiF process (67% for composites, 80% for carbon fiber preform [8]), the fiber alignment is significantly lower here. This is mainly due to: (1) the high pressure applied during the hot compaction forces the matrix to flow out, and hence rotates the fibers (as also noted in [32] when comparing infused and autoclaved composites produced using continuous tapes), (2) PP tape shrinkage, and (3) manual handling of the ADCF performs during the impregnation process.

Since the spatial orientation angle is an overall deviation of fibers from the Z direction, the spatial misalignment is a sum of in-plane misalignment and out-of-plane misalignment. The spatial orientation angle distribution, see Fig. 3b, indicates that only a few percents of the fibers

are aligned within less than 1°. The majority of fibers are misaligned around 10° spatially, while they are preferentially aligned with the 0° direction in-plane. This means that the out-of-plane fiber misalignment is significant in the current study, which can be explained by the relatively thin carbon layer nested in-between woven SRPP layers adopting its crimp.

To estimate the effective modulus of the carbon layer, the fiber volume fraction in the carbon fiber layer is needed. The matrix burn-off tests directly give the overall fiber volume fraction in the hybrid composites, $V_{f,h}$, see Table 2. A back calculation leads to the fiber volume fraction in the carbon layer, $V_{f,CFPP}$, as expressed in Eq. (1),

$$V_{f,CFPP} = \frac{V_{f,h}}{t_{CFPP}/t_h} \tag{1}$$

where $t_{CFPP}$ is the total thickness of the carbon layers in the hybrid composite and $t_h$ is the thickness of the hybrid composite. $t_h$ can be easily measured experimentally by using a micro-meter, while it is not straightforward to measure $t_{CFPP}$ even with optical microscopy. This is because (1) the boundary of the carbon layer is unclear, as the matrices in the carbon layer and SRPP layer are of the same PP grade, and (2) the thickness variation of the carbon layer is significant due to the uneven distribution of carbon fibers and the woven structure of SRPP. Owing to the above difficulties, a different approach to calculate the carbon layer thickness was used. According to our previous work, the thickness of a single SRPP layer, $t_{SRPP}$, is consistently around 0.14 mm, therefore, the thickness of the short carbon fiber layer can be estimated using Eq. (2) while assuming a constant thickness. $n$ is the number of SRPP layers. The estimated carbon layer thicknesses are listed in Table 2.

$$t_{CFPP} = t_h - n \cdot t_{SRPP} \tag{2}$$

Based on the thickness estimates, the carbon fiber volume fraction in the carbon layer, $V_{f,CFPP}$, can be derived using Eq. (1). Also, the modulus of the carbon layer, $E_{CFPP}$, can be calculated using the rule-of-mixtures (ROM), Eq. (3), where $E_h$ and $E_{SRPP}$ are the moduli of the hybrid composite and SRPP (experimental results in Table 3), respectively. The calculated moduli of the carbon layers are summarized in Table 2.

$$E_h \cdot t_h = E_{CFPP} \cdot t_{CFPP} + E_{SRPP} \cdot (t_h - t_{CFPP}) \tag{3}$$

To estimate the effective modulus based on micro-CT results, the carbon fiber layer is assumed to be composed of multiple perfectly aligned short fiber laminas with different orientation angles [34]. The longitudinal modulus of the carbon layer based on micro-CT results, $E_x$, can be calculated as Eq. (4),

$$E_x = \sum_{\alpha} E_x(\alpha) \cdot F(\alpha), \begin{cases} \alpha = \varphi_{ZX}, & \alpha \in [-90°, 90°] \\ \alpha = \theta_{XY}, & \alpha \in [0°, 90°] \end{cases} \quad (4)$$

where $E_x(\alpha)$ is the longitudinal modulus of the short fiber lamina with a certain orientation angle and $F(\alpha)$ is the frequency of the angle in the carbon layer. The detailed calculation of $E_x(\alpha)$ is described in the Appendix and $F(\alpha)$ are plotted in Fig. 3a and 3b. The estimated effective moduli of the short carbon fiber layers based on fiber orientation analysis are plotted together with the experimental results in Fig. 4. Overall, the estimated moduli show a reasonably good agreement with the experimental results. Since the in-plane angle ignores the out-of-plane misalignment that is significant in this study (see Fig. 3b), the moduli based on the in-plane angle calculation of most configurations (except for $S/C^{MAPP}/S$ and $S_2/C^{MAPP}/S_2$) are overestimated. The largest discrepancy is 46.6% for $S_2/C_2^{PP}/S_2$. Comparing to the results based on in-plane fiber orientation, the moduli drop down and get closer to the experimental data when considering spatial misalignment in most configurations except for $S/C^{MAPP}/S$ and $S_2/C^{MAPP}/S_2$. The largest modulus discrepancy in the case of spatial angle is 28.1% for $S_2/C^{MAPP}/S_2$, while the discrepancy is less than 8.3% for $S/C^{PP}/S$, $S/C_2^{PP}/S$, $S/C_3^{PP}/S$, and $C^{PP}/S/C^{PP}/S/C^{PP}$. The reason why the moduli of $S/C^{MAPP}/S$ and $S_2/C^{MAPP}/S_2$ do not obey the trend might be that the scanned specimens were not representative, as the specimens were relatively small. Nevertheless, the above discussion implies that the spatial orientation angle yields a better estimate of the effective modulus of the short carbon fiber layer, as it takes into account both in-plane and out-of-plane fiber misalignment.

### 3.2. Failure mechanisms

Interlayer hybrid composites fail by a number of mechanisms: 1) failure of the low strain material (carbon layer in the current study), 2) delamination (initiated by the low strain material failure) propagation at interlaminar interfaces; and 3) failure of the high strain material (SRPP in

this case) leading to the final failure of the hybrid composite [35]. Moreover, the low strain material can fail either once or multiple times (termed fragmentation). In addition to these ply level (meso-scale) mechanisms, there are also micro-scale failure mechanisms in the carbon layer, including fiber-matrix debonding, fiber breakage and fiber pull-out. The micro-scale failure mechanisms are also present in SRPP layers, for example, in the form of PP tape debonding and matrix cracking, but they are out of the scope of this paper. The meso-scale failure of the carbon layer is a consequence of the micro-scale failure mechanisms taking place there.

The carbon layer failure leads to a significant reduction in the overall stiffness of the hybrid composite, which introduces non-linearity in the stress-strain curve and is displayed as a stress drop or a knee point. Therefore, the stress and strain at carbon layer failure can be extracted from the stress-strain diagram as described in Section 2.3. The stress and strain at carbon layer failure together with the tensile properties of the hybrid composites are summarized in Table 3 and will be used for the following discussion.

*3.2.1. Carbon layer failure*

The failure of a perfectly aligned discontinuous carbon fiber composite can be triggered by either fiber breakage or fiber pull-out depending on the critical fiber length. The critical length can be calculated using the Kelly-Tyson model [36]:

$$L_c = \frac{S \cdot r}{\tau} \tag{5}$$

where $S$ is the strength of the carbon fiber, which is equal to 4344 MPa [8] in the current study, $r$ is the radius of the carbon fiber (3.5 μm), $\tau$ is the interfacial shear strength (IFSS), which is assumed to be 10 MPa for CF/PP and 35 MPa for CF/MAPP [25,37]. Thereby, the critical fiber length is 1.52 mm for CF/PP and 0.43 mm for CF/MAPP, respectively. Since the critical lengths are both significantly lower than the actual fiber length (3 mm), in principal, the carbon fiber should break rather than being pulled out if the fibers are perfectly aligned with the loading direction. However, in practice, the fibers are misaligned both in-plane and out-of-plane as discussed in Section 3.1. They are hence also loaded off-axis and the off-axis load produces a normal peeling stress at the fiber-matrix interface promoting fiber-matrix debonding and fiber pull-out. With better fiber alignment in the loading direction, the micro-scale failure in the carbon

layer can experience a transition from pure fiber pull-out to pure fiber breakage with a combination of both in between, see Fig. 5. Since the fiber orientation angle exhibits a relatively wide range, as shown in Fig. 3b, the above three micro-scale failure mechanisms should all co-exist in the carbon layer. Based on the SEM images of the fracture surface shown in Fig. 6a and b, the fibers are mainly pulled out irrespective of the fiber-matrix interface being CF/PP or CF/MAPP, though it is difficult to distinguish carbon fiber breakage based on the fractography. The fiber pull-out can be proven by the following evidence: (1) the pull-out length is much longer compared to the pull-out length when carbon fibers break in the case of strong interfacial bonding; (2) the strain at carbon layer failure is around 1% (see Table 3) that is much lower than the failure strain of the carbon fiber (around 1.9% [13]), and (3) the majority of fibers have a spatial orientation angle around 10º as shown in Fig. 3b.

As shown in Fig. 6c and d, the carbon fiber surface is relatively clean for CF/PP, while there are still matrix residues bonded onto the carbon fiber in the case of CF/MAPP. This indicates that CF/MAPP has a stronger interface than CF/PP created by the chemical bonding, which is in line with the findings in Karsli et al. [24]

*3.2.2. Carbon layer fragmentation*

The accumulation of the microscopic failure leads to the ply-level carbon layer failure, which can happen once or multiple times in the hybrid composite. In continuous CF/SRPP hybrids, the carbon layer failure is attributed to fracture of carbon fibers, which releases strain energy in an abrupt way and results in an instantly formed delamination with a certain length [21,22]. Thanks to the translucency of the SRPP layers, the carbon layer failure can be easily detected. Thus once the delamination occurs, it changes the way the light passes through the specimen and hence appears white to the observer [22]. However, in the case of discontinuous fiber composites, the carbon layer failure is mainly triggered by fiber/matrix debonding and fiber pull-out and the energy is dissipated in a more gradual way than in the case of fiber breakage. The resulting delamination is so small that it is more difficult to detect visually than the abruptly formed large-scale delamination upon carbon layer failure in continuous CF/SRPP hybrids. Moreover, the specimen surface was fully speckled for DIC during the tensile test, which made detection of the

initial delamination induced by carbon layer failure even more difficult. Nevertheless, once the carbon layer fails, the stress is transferred to the neighboring SRPP layers, thereby increasing the strain in the SRPP layers, and this strain magnification can be studied by means of DIC on the specimen surface.

Fig.7 demonstrates an example of local strain evolution along with the carbon layer in $S/C^{PP}/S$. The strain localization on the strain map (see Fig. 7a) indicates the region of delamination caused by the carbon layer failure. Looking at the longitudinal strain evolution along the path, see Fig. 7b, there is no carbon layer failure when the applied strain is 1%. There might be local carbon layer failure at the edges, as the strain at the carbon layer failure for $S/C^{PP}/S$ in Table 3 is slightly lower than 1% meaning the carbon layer failure has already onset. The local failure at the edges can be captured by the full strain map instead of the strain distribution along the line path, as the current line path is in the middle of the specimen and only captures the strain localization on it. The strain periodicity with a length of around 4 mm at an applied strain of 1% is caused by the woven structure of the SRPP [38]. The peaks correspond to the location in between weft yarns, where the warp yarns are crimped and there are resin pockets, see Fig. 7c. Upon further increase of the applied strain, a sudden magnification of local strain appears at multiple locations. The sudden increase in local strain is attributed to carbon layer failure developing across the line path, with the number of strain peaks indicating how many times the carbon layer fails. The carbon layer is therefore fragmenting.

Carbon layer fragmentation was detected in $S/C^{PP}/S$ and $S_2/C_2^{PP}/S_2$, while the carbon layer failed only once in other layups. The critical carbon layer thickness, $t_{CFPP}^{C}$, for achieving fragmentation in interlayer hybrid composites satisfies the following equation [39]:

$$G_{IIC} = \frac{\sigma_{CFPP}^2 \cdot t_{CFPP}^{C} \cdot (E_{SRPP} \cdot (t_h - t_{CFPP}^{C}) + E_{CFPP} \cdot t_{CFPP}^{C})}{4 \cdot E_{SRPP} \cdot E_{CFPP} \cdot (t_h - t_{CFPP}^{C})} \quad (6)$$

where $G_{IIC}$ is the mode II interlaminar fracture toughness for propagation and $\sigma_{CFPP}$ is the strength of the carbon layer. This calculation assumes that the delamination is the only energy-consuming mechanism [39]. If the carbon layer thickness is below the critical value, $t_{CFPP}^{C}$, the energy released at carbon layer failure is not enough to promote delamination propagation and

the carbon layer tends to fragment. This equation only works for the interlayer hybrid structure with low elongation materials (carbon fiber layers in this study) centralized in the middle. The dispersed layup $C^{PP}/S/C^{PP}/S/C^{PP}$ is therefore not included in the calculation. $\sigma_{CFPP}$ can be estimated using Eq. (7),

$$\sigma_{CFPP} = \frac{\sigma^* \cdot t_h - E_{SRPP} \cdot \varepsilon^* \cdot (t_h - t_{CFPP})}{t_{CFPP}} \quad (7)$$

where $\sigma^*$ and $\varepsilon^*$ are the stress and strain at the carbon layer failure summarized in Table 3.

Since the aligned discontinuous carbon fiber reinforced PP is not a common material, its $G_{IIC}$ has not been reported yet in the literature. Chen [40] reported an interlaminar fracture toughness of 0.214 ± 0.025 kJ/m$^2$ for continuous CF/SRPP hybrids, where the PP matrix was the same as the one used in the current study. It is noted that this value is the interlaminar fracture toughness for initiation, which is normally lower than that for propagation. The other value of $G_{IIC}$ for carbon fiber reinforced PP composites reported in the literature was 0.518 kJ/m$^2$ [21]. It was measured for continuous carbon fiber/PP laminates, where the PP matrix is different from the one used in this study. Several caveats have to be emphasized here:

(1) The fiber type in Chen [40] is Toray T700S, while the fiber type here is Tenax C124. This means that fiber/matrix adhesion is likely to be different, which would also affect the interlaminar fracture toughness;

(2) All values found in the literature were for continuous fibers. The lack of fiber continuity may further influence the interlaminar fracture toughness.

(3) The interlaminar fracture toughness for CF/MAPP was not found in the literature.

Despite all the difficulties in getting accurate values for $G_{IIC}$, the calculation of the critical thickness as a function of $G_{IIC}$ is still a useful exercise. The results of such a calculation are shown in Fig. 8. If the actual carbon layer thickness is below the critical layer thickness, then the carbon layer will fragment. As demonstrated in Fig. 8, the actual layer thicknesses of $S/C^{PP}/S$ and $S_2/C_2^{PP}/S_2$ are lower than their corresponding critical thicknesses within the range of reported interlaminar fracture toughness for CF/PP, while the actual thicknesses of $S/C_2^{PP}/S$ and $S/C_3^{PP}/S$ are higher than the critical thicknesses. Therefore, the carbon layer should fragment for the first

two layups, while there should be no fragmentation for the latter two layups. This corresponds well to the experimental results and indicates that the ply-level critical thickness criterion can be successfully applied to discontinuous fiber hybrids. In summary, though the micro-scale damage mechanisms are different, the higher-level structural parameters still govern the global failure behavior of interlayer hybrid composites.

Furthermore, increasing the ratio of carbon/SRPP layers by adding more carbon layers in the middle does not greatly alter the critical thickness, but increases the absolute carbon layer thickness significantly. This makes the actual layer thickness higher than the critical thickness, hence resulting in no carbon layer fragmentation.

Changing the matrix from PP to MAPP significantly reduces the critical thickness. This means a thinner carbon layer is required to achieve carbon layer fragmentation with MAPP than with PP. Due to the missing value for the interlaminar fracture toughness, it is difficult to compare the critical thickness and the actual thickness in this case.

*3.2.3. Delamination and SRPP layers failure*

As a consequence of carbon layer failure, either once or multiple times, the delamination can be initiated at the interface between the carbon and SRPP layers. Ductility of the hybrid composites is closely linked to the delamination propagation. More specifically, if the delamination is allowed to grow more extensively before SRPP failure, then the hybrid composite ends up being more ductile (higher failure strain). Fig. 9 reveals that the SRPP layers are found to fail prematurely in most cases, where the delamination propagation is quite limited. A fully extended delamination is observed in $S/C^{PP}/S$, $S_2/C_2^{PP}/S_2$ and a local delamination is found in $S_2/C^{MAPP}/S_2$. This corresponds well to the fact that the ultimate failure strains of $S/C^{PP}/S$ and $S_2/C_2^{PP}/S_2$ are much higher than those of other layups, see Table 3. The premature failure of SRPP layers is caused by too much stress being shifted to them after the failure of the carbon layer. At the moment of carbon layer failure, the stress, $\sigma_{SRPP}^{*}$, in the SRPP layers at the cross-section where the carbon layer has failed, can be calculated using Eq. (8), ignoring any stress concentration.

$$\sigma^*_{SRPP} = \frac{\sigma^* \cdot t_h}{t_h - t_{CFPP}} \quad (8)$$

The results are plotted in Fig. 10. Compared to the strength of SRPP, the stress is too high for the SRPP layers to sustain after carbon layer failure in layups $S/C_2^{PP}/S$, $S/C_3^{PP}/S$, $C^{PP}/S/C^{PP}/S/C^{PP}$ and $S/C^{MAPP}/S$. Therefore, the SRPP layers fail shortly after the carbon layer failure. As for the other layups, $\sigma^*_{SRPP}$ is lower than the strength of SRPP, which allows SRPP layers to continue carrying load after carbon layer failure and allows delamination to propagate. This analysis is supported by experimental observations, as shown in Fig. 9.

### 3.3. Effect of design parameters on the tensile behavior

In this section, the effects of the design parameters, including carbon layer thickness, carbon/SRPP thickness ratio, layer dispersion and interfacial properties, on the failure mechanisms and thereby the tensile behavior of the hybrid composites will be analyzed. Based on the observation in Section 3.2, different ply-level failure mechanisms for each hybrid layup are summarized in Table 4. The representative stress-strain diagrams of all the layups are plotted in Fig. 11a. The table and figure will be used for the discussion below. Besides, the trade-off between modulus and ultimate failure strain is demonstrated in Fig. 11b.

Increasing the carbon layer thickness while keeping the same ratio of carbon/SRPP layers does not alter the failure mechanisms of $S/C^{PP}/S$ and $S_2/C_2^{PP}/S_2$, as they both fail by carbon layer fragmentation accompanied with dispersed delamination growth, see Table 4. Both layups demonstrate a gradual failure with a smooth transition in stress-strain diagrams (black and blue solid line in Fig. 11a. This is different from what has been found for continuous CF/SRPP hybrids [21, 22], which exhibited stress drops in the stress-strain diagrams when carbon layer fragmented. This is because the carbon layer fails differently in these hybrids, more specifically by fiber fracture in continuous CF/SRPP hybrids, and by mainly fiber pull-out in ADCF/SRPP hybrids. As a result, the delamination always forms suddenly with a certain length in continuous CF/SRPP hybrids while it forms only locally in ADCF/SRPP hybrids. Therefore, a much smoother transition is observed in the stress-strain diagrams for ADCF/SRPP hybrids. To demonstrate the gradual failure behavior, a pseudo-ductile strain can be used. It is defined as the difference

between the elastic strain at the maximal stress based on the initial modulus and the ultimate failure strain [41]. In this case, the pseudo-ductile strain is calculated to be high, 13.1% ± 4.4% for $S/C^{PP}/S$ and 11.5% ± 2.9% for $S_2/C_2^{PP}/S_2$. This is much higher than that for continuous (or discontinuous) carbon/glass hybrids, which has been reported as up to 2.64% [20,41,42].

Increasing the carbon fiber volume fraction while keeping the same carbon layer thickness turns the hybrid composites from being ductile to brittle (see $S_2/C_2^{PP}/S_2$ and $S/C_2^{PP}/S$ in Fig. 11a). By decreasing the number of SRPP layers above and below the carbon layer, the ratio of carbon/SRPP layers is increased. Hence, a higher stress is transferred from the carbon layer to the neighboring SRPP layers when the carbon layer fails. As shown in Fig. 10, the stress in the SRPP layers at the cross section of carbon layer failure is higher than the strength of SRPP in $S/C_2^{PP}/S$. Therefore, the SRPP layers fail shortly after the failure of carbon layer.

Comparing the stress-strain diagram of $S/C_3^{PP}/S$ and $C^{PP}/S/C^{PP}/S/C^{PP}$, the dispersed layup of carbon layer does not help to maintain ductility of the hybrids. In principle, dispersing the carbon fiber layers should increase ductility of the hybrid composites, as more interfaces of carbon and SRPP layers are created for energy dissipation [43]. However, the hybrids fail right after the failure of the carbon layer for both $C^{PP}/S/C^{PP}/S/C^{PP}$ and $S/C_3^{PP}/S$. This is because the SRPP layers cannot sustain the stress shifted from the carbon layer when it fails, as shown in Fig. 10. In conclusion, the dispersion strategy does not work if the thickness ratio of carbon/SRPP layers is too high.

By comparing $S/C^{PP}/S$ versus $S/C^{MAPP}/S$ in Fig. 11a, it can be seen that simply modifying the matrix from PP to MAPP turns a ductile hybrid into a brittle one. Although the thickness ratio of carbon/SRPP layers is identical for both layups, the applied stress at carbon layer failure is much higher for $S/C^{MAPP}/S$, see Table 3. Hence, a much higher stress in the SRPP layers after carbon layer failure is expected for $S/C^{MAPP}/S$, as shown in Fig. 10. The increased stress at carbon layer failure is mainly attributed to two factors. Firstly, the modulus of the CF/MAPP layer is higher than the modulus of the CF/PP layer (see Table 2), which is due to the higher fiber volume fraction in the CF/MAPP as shown in Table 2. The reason for this higher volume fraction

is not known, but likely due to inherent production variations. Secondly, the CF/MAPP layer fails later than the CF/PP layer (see strain at carbon layer failure in Table 3), which is due to the better interfacial properties delaying the onset of fiber-matrix debonding [24].

Decreasing the thickness ratio of the carbon/SRPP layers by adding more SRPP layers (see $S/C^{MAPP}/S$ versus $S_2/C^{MAPP}/S_2$ in Fig. 11a) significantly reduces the stress shifted to the SRPP layers at carbon layer failure, see Fig. 10. This allows the SRPP layers to continue their elongation after carbon layer failure, which explains the higher failure strain of $S_2/C^{MAPP}/S_2$ (see Table 3).

**4. Conclusions**

This paper introduced a novel hybrid composite that consists of aligned discontinuous carbon fibers and self-reinforced polypropylene. With the best laminate design, the hybrid composite demonstrates a graceful deformation up to failure in combination with a stiffness of around 10 GPa and a failure strain up to 14%. More than 10% pseudo-ductile strain is obtained for this hybrid composite. Compared to the 3 GPa stiffness and 20% failure strain of SRPP, the stiffness is over three times higher with still relatively high ductility. This means that the developed hybrid composite has a more balanced mechanical performance. More importantly, the gradual failure with more than 10% pseudo-ductile strain provides warning before final failure of the hybrid composite, which is vital for safety management in real-life applications. Since SRPP has been successfully applied in many commercial products, such as suitcases, helmets and rackets [44], the developed hybrid composites can be used as a replacement of SRPP in such applications.

In comparison with continuous CF/SRPP hybrids, which suffer from sudden stress drops on the stress-strain diagram, the ADCF/SRPP composite exhibits a much smoother transition when the carbon layer fragments. However, to achieve this in interlayer ADCF/SRPP hybrid composites, the criteria developed for continuous fiber-hybrids, including the critical thickness for achieving layer fragmentation and the minimum high elongation material strength to avoid premature failure, are still applicable for the discontinuous fiber-hybrids. This means that the ply-level failure mechanisms dominate the tensile behavior of interlayer hybrid composites despite the difference in microscopic failure mechanisms. In both continuous and discontinuous fiber-hybrids, low

elongation material fragmentation is the key for achieving a gradual deformation up to failure under tensile loading.

The alignment of the discontinuous fibers in the hybrid composite could be significantly affected by processing conditions as well as texture of the outer layer materials. The high pressure and temperature in composite production allowed the discontinuous fibers to flow and distort, which led to their misalignment. Also, the ductile SRPP printed its woven structure onto the carbon fiber layer under high pressure, which further affected the fiber alignment. Furthermore, the alignment of the discontinuous fibers is crucial for the layer modulus and can be efficiently characterized using X-ray computed tomography.

Compared to conventional carbon/glass hybrids, the high ductility of SRPP in the ADCF/SRPP hybrid composite allows larger elongation of the hybrid composite, and hence creates greater pseudo-ductility in the case of low elongation layer fragmentation.

**Acknowledgements**

Jun Tang would like to acknowledge China Scholarship Council for supporting his PhD study at KU Leuven. Yentl Swolfs acknowledges FWO Flanders for his postdoctoral fellowship. S.V. Lomov holds the Toray Chair in Composite Materials at KU Leuven, support of which is gratefully acknowledged. The work conducted at the University of Bristol was supported by the UK Engineering and Physical Sciences Research Council through the project "High Performance Discontinuous Fibre Composites – a sustainable route to the next generation of composites" (Grant number EP/P027393/1).

**Appendix**

The longitudinal modulus of a unidirectional short fiber lamina, $E_1$, can be calculated using a modified rule of mixture, Eq. (A1).

$$E_1 = \eta \cdot E_{f1} \cdot V_{f,CFPP} + E_{PP} \cdot (1 - V_{f,CFPP}) \quad \text{(A1)}$$

Here, $E_{f1}$ is the longitudinal modulus of the carbon fiber and $E_{PP}$ is the modulus of the matrix (listed in Table 1), $\eta$ is the fiber length efficiency factor for short fiber composites and can be estimated with shear lag theory (Cox's model [45]), as expressed in Eq. (A2)

$$\eta = 1 - \frac{\tanh(\beta \cdot l\,/\,d)}{\beta \cdot l\,/\,d} \tag{A2}$$

with

$$\beta = \sqrt{\frac{2 \cdot G_{PP}}{E_{f1} \cdot \ln(\sqrt{\pi / V_{f,CFPP}})}} \tag{A3}$$

$l$ and $d$ are the fiber length and diameter respectively. $G_{PP}$ is the shear modulus of the matrix. Assuming that the longitudinal Poisson's ratio $\nu_{12}$ is not sensitive to fiber length, it can be calculated with the linear rule-of-mixture, as Eq. (A4). $\nu_{f12}$ and $\nu_{PP}$ are the Poisson's ratios of the carbon fiber and matrix, respectively.

$$\nu_{12} = \nu_{f12} \cdot V_{f,CFPP} + \nu_{PP} \cdot (1 - V_{f,CFPP}) \tag{A4}$$

The transverse modulus, $E_2$, and in-plane shear modulus, $G_{12}$, are barely affected by fiber length [34]. In the current study, they are estimated using Chamis' formulas [46], as described in Eq. (A5) and (A6). $E_{f2}$ is the transverse modulus of the carbon fiber and $G_{f12}$ is the shear modulus of the carbon fiber.

$$E_2 = \frac{E_{PP}}{1 - \sqrt{V_{f,CFPP}} \cdot (1 - E_{PP}/E_{f2})} \tag{A5}$$

$$G_{12} = \frac{G_{PP}}{1 - \sqrt{V_{f,CFPP}} \cdot (1 - G_{PP}/G_{f12})} \tag{A6}$$

Taking into account the fiber orientation, the longitudinal modulus of the lamina with a certain angle, $E_x(\alpha)$, can be estimated with classical laminate theory (CLT), as expressed in Eq. (A7).

$$\frac{1}{E_x(\alpha)} = \frac{\cos^4 \alpha}{E_1} + \frac{\cos^2 \alpha \cdot \sin^2 \alpha}{(1/G_{12} - 2\nu_{12}\,/\,E_1)} + \frac{\sin^4 \alpha}{E_2} \tag{A7}$$

**References**


[1] Harper LT. Discontinuous Carbon Fibre Composites for Automotive Applications. PhD thesis, the University of Nottingham, 2006.

[2] Nishikawa M, Okabe T, Takeda N. Periodic-Cell Simulations for the Microscopic Damage and Strength Properties of Discontinuous Carbon Fiber-Reinforced Plastic Composites. Adv Compos Mater 2009;35:149–56.

[3] Lei HF, Zhang ZQ, Liu B, Chen B, Wu PD, Gao H. Effect of fiber arrangement on mechanical properties of short fiber reinforced composites. Compos Sci Technol 2012;72:506–14.

[4] Hashimoto M, Okabe T, Sasayama T, Matsutani H, Nishikawa M. Prediction of tensile strength of discontinuous carbon fiber/polypropylene composite with fiber orientation distribution. Compos Part A Appl Sci Manuf 2012;43:1791–9.

[5] Ericson ML, Berglund LA. Processing and mechanical properties of orientated preformed glass-mat-reinforced thermoplastics. Compos Sci Technol 1993;49:121–30.

[6] Papathanasiou TD, Guell DC. Flow-induced Alignment in Composite Materials. England: Woodhead; 1997.
[7] Salariya AK, Pittman JFT. Preparation of aligned discontinuous fiber pre-pregs by deposition from a suspension. Polym Eng Sci 1980;20:787–97.
[8] Yu H, Potter KD, Wisnom MR. A novel manufacturing method for aligned discontinuous fibre composites (High Performance-Discontinuous Fibre method). Compos Part A Appl Sci Manuf 2014;65:175–85.
[9] Longana ML, Yu HN, Jalavand M, Wisnom MR, Potter KD. Aligned discontinuous intermingled reclaimed/virgin carbon fibre composites for high performance and pseudo-ductile behaviour in interlaminated carbon-glass hybrids. Compos Sci Technol 2017;143:13–21.
[10] Longana ML, Ong N, Yu HN, Potter KD. Multiple closed loop recycling of carbon fibre composites with the HiPerDiF (High Performance Discontinuous Fibre) method. Compos Struct 2016;153:271–7.
[11] Tapper R, Longana ML, Yu H, Hamerton I, Potter PK. Development of a closed-loop recycling process for short carbon fibre polypropylene composites. Compos Part B Eng 2018;146:222–31.
[12] Longana ML, Ondra V, Yu H, Potter KD, Hamerton I. Reclaimed Carbon and Flax Fibre Composites : Manufacturing and Mechanical Properties. Recycling 2018;3:1–13.
[13] Yu H, Longana ML, Jalalvand M, Wisnom MR, Potter KD. Pseudo-ductility in intermingled carbon/glass hybrid composites with highly aligned discontinuous fibres. Compos Part A Appl Sci Manuf 2015;73:35–44.
[14] Longana ML, Yu H, Hamerton I, Potter KD. Development and application of a quality control and property assurance methodology for reclaimed carbon fibers based on the HiPerDiF ( High Performance Discontinuous Fibre ) method and interlaminated hybrid specimens. Adv Manuf Polym Compos Sci 2018;4:48–55.
[15] Yu H, Longana ML, Grail G, Pimenta S, Robinson P, Wisnom MR, Potter KD. Aligned Short Fibre Composites With Nonlinear Behaviour. 20th Int. Conf. Compos. Mater., 2015.
[16] Swolfs Y, Gorbatikh L, Verpoest I. Fibre hybridisation in polymer composites: A review. Compos Part A Appl Sci Manuf 2014;67:181–200.
[17] Swolfs Y, Verpoest I, Gorbatikh L. Recent advances in fibre-hybrid composites : materials selection , opportunities and applications. Int Mater Rev 2018:1–35.
[18] Fu S, Lauke B, Edith M a. Hybrid effects on tensile properties of hybrid short-glass-fiber- and short-carbon-fiber- reinforced polypropylene composites. Adv Mater 2006;6:1243–51.
[19] Finley J, Yu H, Longana ML, Pimenta S, Shaffer MSP, Potter KD. Exploring the pseudo-ductility of aligned hybrid discontinuous composites using controlled fibre-type arrangements. Compos Part A Appl Sci Manuf 2017;107:592–606.
[20] Yu H, Longana ML, Jalalvand M, Wisnom MR, Potter KD. Hierarchical pseudo-ductile hybrid composites combining continuous and highly aligned discontinuous fibres. Compos Part A Appl Sci Manuf 2018;105:40–56.
[21] Swolfs Y, Meerten Y, Hine P, Ward I, Verpoest I, Gorbatikh L. Introducing ductility in hybrid carbon fibre/self-reinforced composites through control of the damage mechanisms. Compos Struct 2015;131:259–65.
[22] Tang J, Swolfs Y, Yang M, Michielsen K, Ivens J, Lomov SV, Gorbatikh L. Discontinuities as a way to influence the failure mechanisms and tensile performance of hybrid carbon fiber/self-reinforced polypropylene composites. Compos Part A Appl Sci Manuf 2018;107:354–65.
[23] Hirano N, Muramatsu H, Inoue T. Study of fiber length and fiber-matrix adhesion in carbon-fiber-reinforced polypropylenes. Adv Compos Mater 2014;23:151–61.
[24] Karsli NG, Aytac A. Effects of maleated polypropylene on the morphology, thermal and mechanical properties of short carbon fiber reinforced polypropylene composites. Mater Des 2011;32:4069–73.
[25] Burn DT, Harper LT, Johnson M, Warrior NA, Nagel U, Yang L, Thomason J. The usability of recycled carbon fibres in short fibre thermoplastics: interfacial properties. J

Mater Sci 2016;51:7699–715.
[26] Swolfs Y, Zhang Q, Baets J, Verpoest I. The influence of process parameters on the properties of hot compacted self-reinforced polypropylene composites. Compos Part A Appl Sci Manuf 2014;65:38–46.
[27] Mehdikhani M, Gorbatikh L, Verpoest I, Lomov S V. Voids in fiber-reinforced polymer composites: A review on their formation, characteristics, and effects on mechanical performance. J Compos Mater 2018;53:1579–669.
[28] Swolfs Y, Shi J, Meerten Y, Hine P, Ward I, Verpoest I, Gorbatikh L. The importance of bonding in intralayer carbon fibre/self-reinforced polypropylene hybrid composites. Compos Part A Appl Sci Manuf 2015;76:299–308.
[29] Shen H, Nutt S, Hull D. Direct observation and measurement of fiber architecture in short fiber-polymer composite foam through micro-CT imaging. Compos Sci Technol 2004;64:2113–20.
[30] Bernasconi A, Cosmi F, Hine PJ. Analysis of fibre orientation distribution in short fibre reinforced polymers : A comparison between optical and tomographic methods. Compos Sci Technol 2012;72:2002–8.
[31] Binh T, Thi N, Morioka M, Yokoyama A, Hamanaka S. Journal of Materials Processing Technology Measurement of fiber orientation distribution in injection-molded short-glass-fiber composites using X-ray computed tomography. J Mater Process Tech 2015;219:1–9.
[32] Nguyen NQ, Mehdikhani M, Straumit I, Gorbatikh L, Lessard L, Lomov S V. Micro-CT measurement of fibre misalignment: Application to carbon/epoxy laminates manufactured in autoclave and by vacuum assisted resin transfer moulding. Compos Part A Appl Sci Manuf 2018;104:14–23.
[33] Straumit I, Lomov S V, Wevers M. Quantification of the internal structure and automatic generation of voxel models of textile composites from X-ray computed tomography data. Compos Part A 2015;69:150–8.
[34] Fu SY, Hu X, Yue CY. The elastic modulus of misaligned short-fiber-reinforced polymers. Compos Sci Technol 1999;59:1533–42.
[35] Jalalvand M, Czél G, Wisnom MR. Damage analysis of pseudo-ductile thin-ply UD hybrid composites – A new analytical method. Compos Part A Appl Sci Manuf 2015;69:83–93.
[36] Kelly A, Tyson WR. Tensile properties of fibre-reinforced metals: Copper/tungsten and copper/molybdenum. J Mech Phys Solids 1965;13:329–50.
[37] Nakamura H, Tanaka Y, Nakai A, Kobayashi S, Ikuta N. Interfacial Properties of Carbon Fiber reinforced thermoplastic composites. 10th Int. Conf. flow Process. Compos. Mater., 2010.
[38] Tabatabaei SA, Swolfs Y, Wu H, Lomov S V. Full-field strain measurements and meso-FE modelling of hybrid carbon/self-reinforced polypropylene. Compos Struct 2015;132:864–73.
[39] Czél G, Wisnom MR. Demonstration of pseudo-ductility in high performance glass/epoxy composites by hybridisation with thin-ply carbon prepreg. Compos Part A Appl Sci Manuf 2013;52:23–30.
[40] Chen B. Characterization of the interlaminar fracture toughness of hybrid carbon fibre / self-reinforced polypropylene composites to support model development. Master thesis, KU Leuven, 2018.
[41] Czél G, Jalalvand M, Wisnom MR. Design and characterisation of advanced pseudo-ductile unidirectional thin-ply carbon/epoxy-glass/epoxy hybrid composites. Compos Struct 2016;143:362–70.
[42] Czél G, Jalalvand M, Wisnom MR. Demonstration of pseudo-ductility in unidirectional hybrid composites made of discontinuous carbon/epoxy and continuous glass/epoxy plies. Compos Part A Appl Sci Manuf 2015;72:75–84.
[43] Selezneva M, Swolfs Y, Katalagarianakis A, Ichikawa T, Hirano N, Taketa I, Karaki T, Verpoest I, Gorbatikh L. The brittle-to-ductile transition in tensile and impact behavior of hybrid carbon fibre/self-reinforced polypropylene composites. Compos Part A Appl Sci Manuf 2018;109:20–30.
[44] Propex. Applications of SRPP n.d. https://www.curvonline.com/products-

services/applications.html.
[45] Cox HL. The elasticity and strength of paper and other fibrous materials. Br J Appl Phys 1952;3:72–9.
[46] Chamis CC. Mechanics of Composite Materials : Past , Present , and Future. J Compos Technol Res 1989;11:3–14.

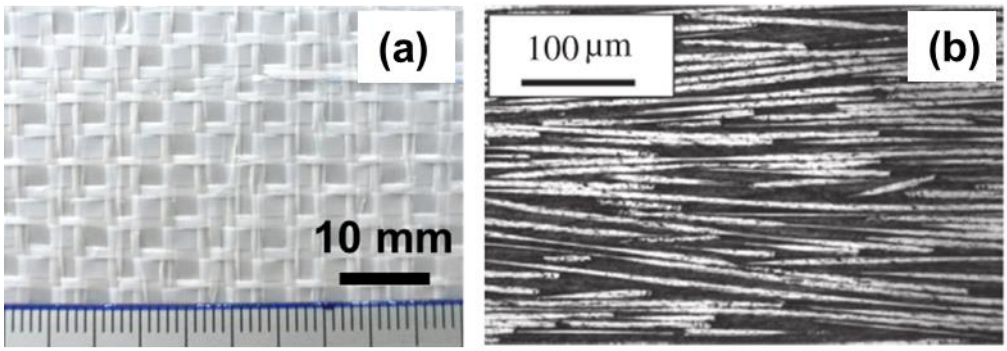


Fig. 1. Raw materials: (a) PP tape fabric for production of self-reinforced polypropylene, and (b) aligned discontinuous carbon fiber preform (reprinted from [8], with permission from Elsevier).

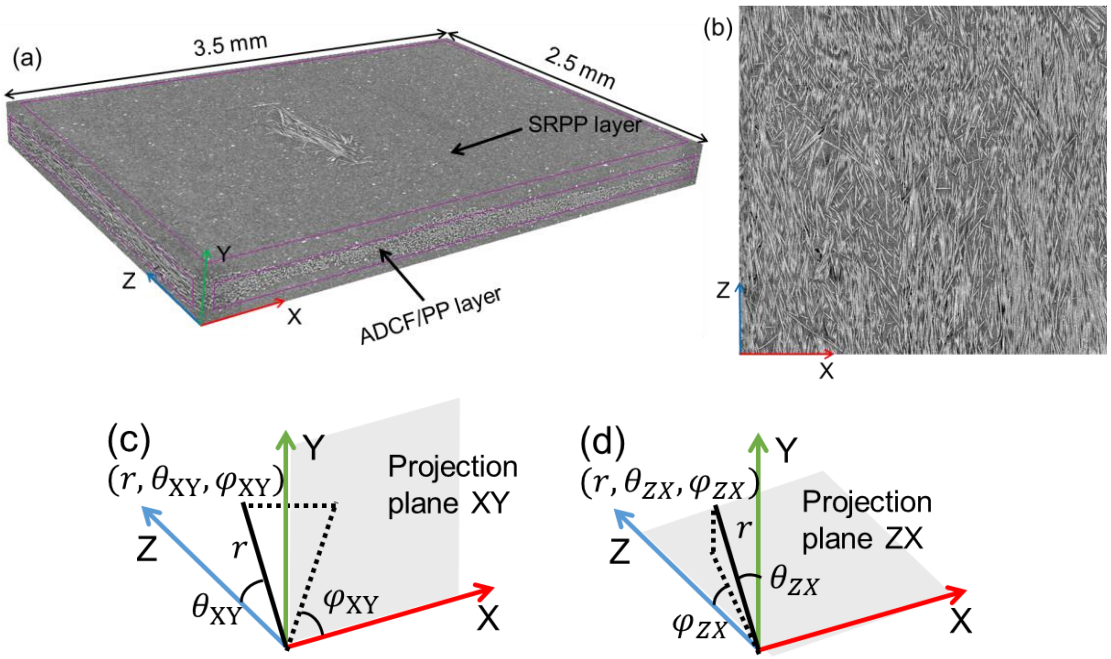


Fig. 2. Micro-CT images of a (a) cut-out volume of the specimen, (b) slice of ZX plane indicating in-plane fiber orientation of the short carbon fibers and low void content in the carbon fiber layer. Definition of (c) spatial orientation angle, $\theta_{XY}$, and (d) in-plane orientation angle, $\varphi_{ZX}$.

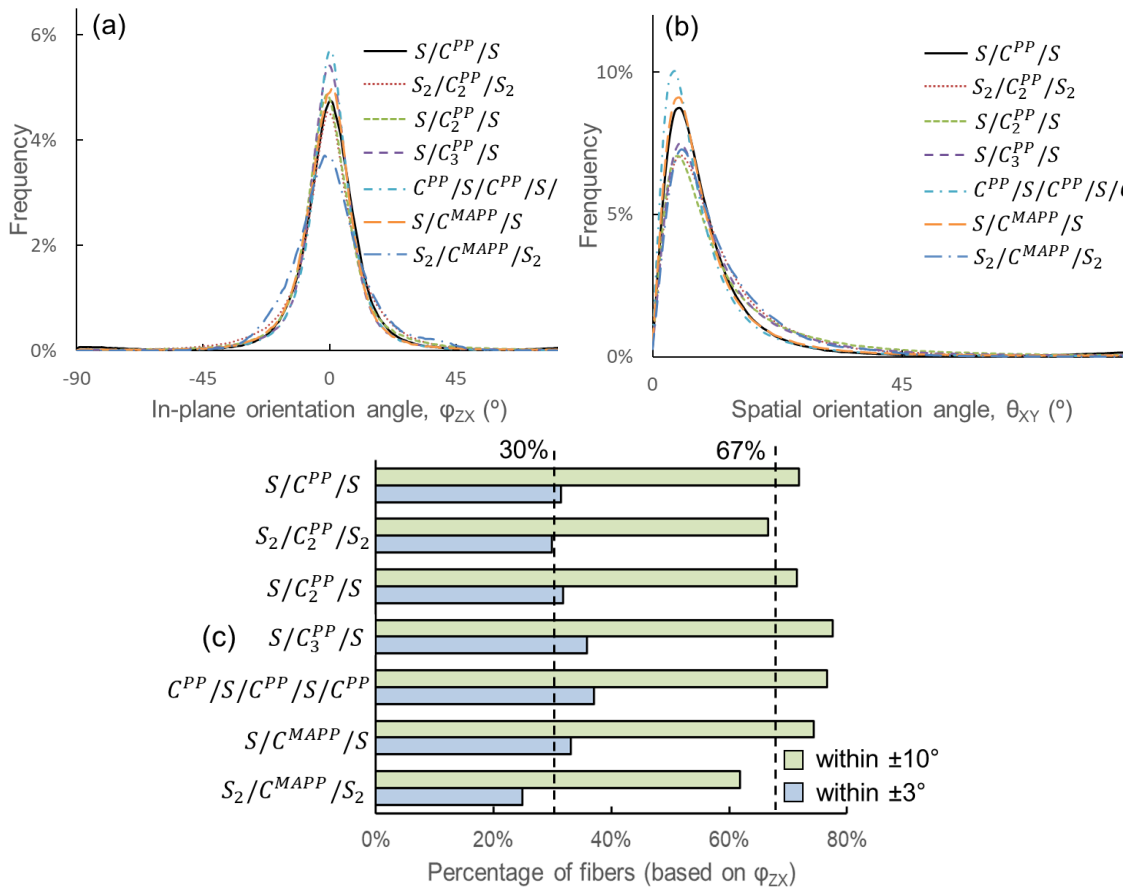


Fig. 3. Carbon fiber orientation distribution in hybrid composites: (a) in-plane angle, $\varphi_{ZX}$, (b) spatial angle, $\theta_{XY}$, and (c) percentage of fibers within ± 3° and within ± 10° based on $\varphi_{ZX}$.

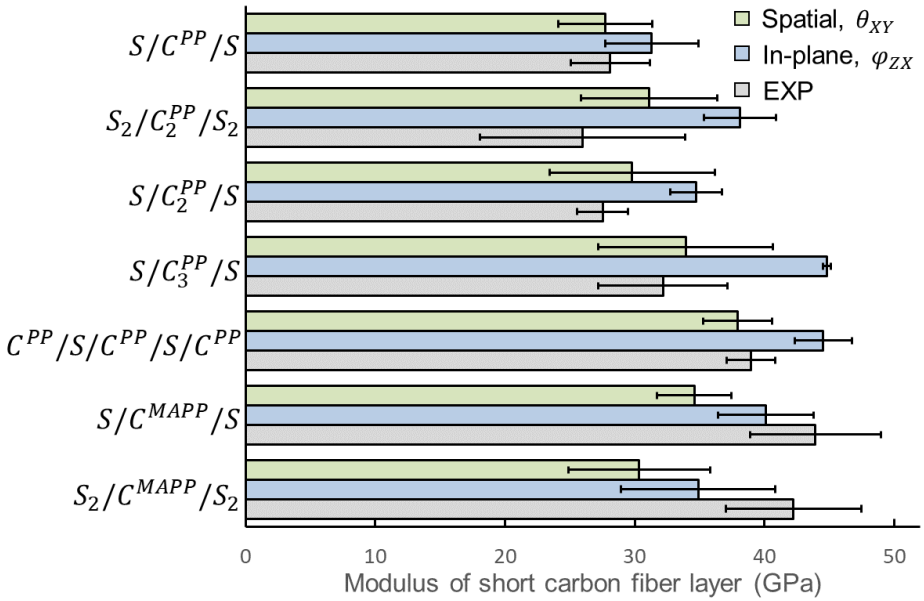


Fig. 4. Predictions of longitudinal modulus of the short carbon fiber layer and fiber orientation distribution (in-plane and spatial) in comparison with experimental results (EXP).

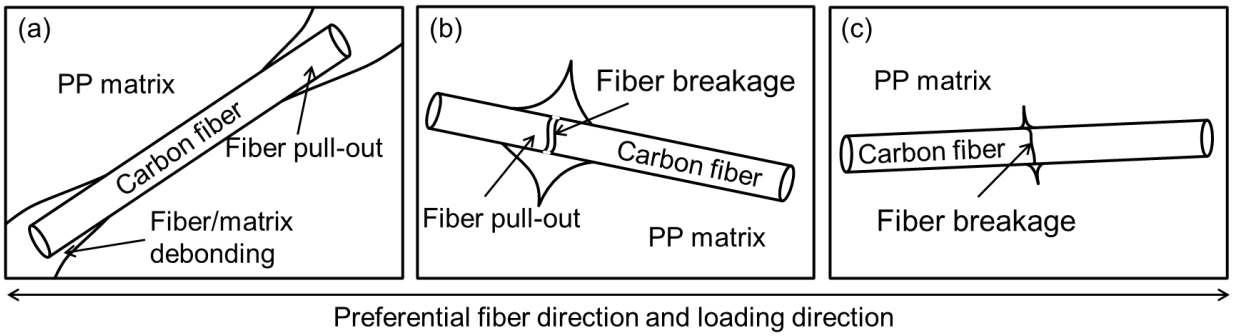


Fig. 5. Schematics of possible micro-scale failure mechanisms in the carbon layer: (a) carbon fiber pull-out, (b) carbon fiber breakage followed by fiber pull-out, and (c) carbon fiber breakage.

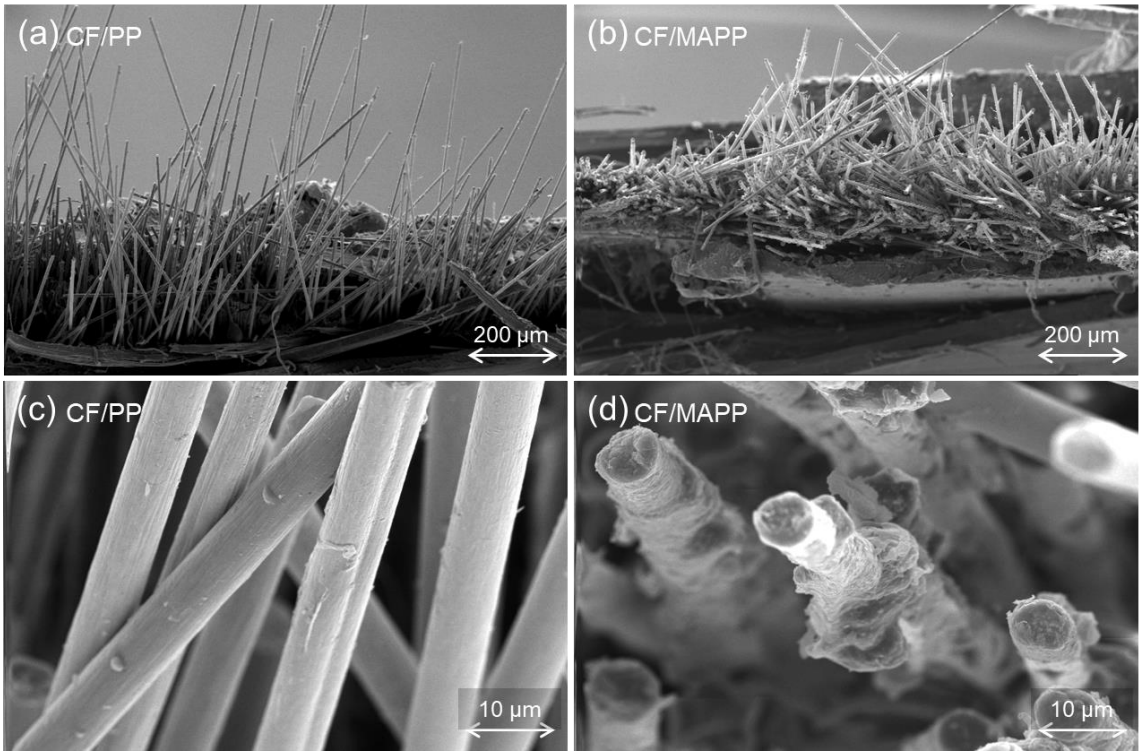


Fig. 6. SEM images of fiber pull-out in (a) CF/PP and (b) CF/MAPP and SEM images of fiber surface in (c) CF/PP and (d) CF/MAPP showing a better interfacial bonding in CF/MAPP.

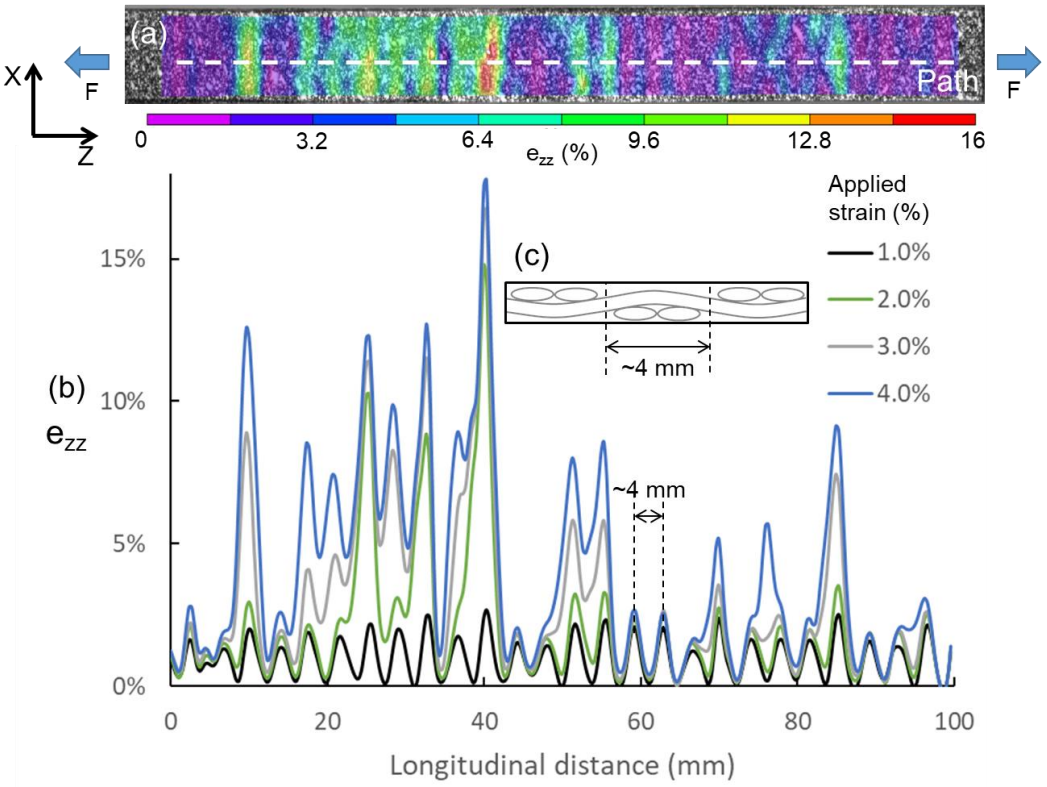


Fig. 7. (a) Strain map on the specimen surface at an applied strain of 4.0%, (b) longitudinal strain ($e_{xx}$) distribution along the specimen length at different applied strains indicating carbon layer fragmentation, and (c) schematics of the woven structure of SRPP accounting for the strain periodicity when applied strain is 1.0%.

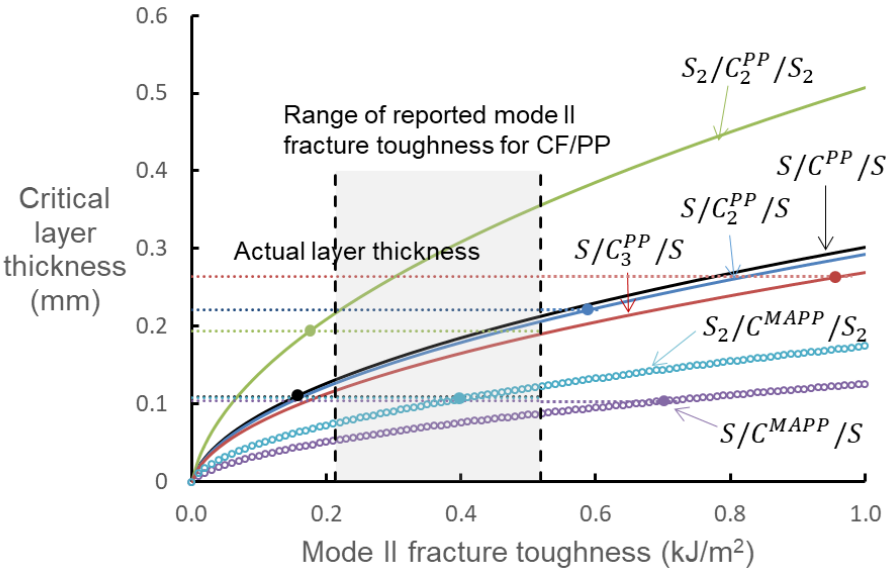


Fig. 8. Predictions (solid lines and circled scatters) of the critical carbon layer thickness for achieving fragmentation together with the actual carbon layer thickness (dashed lines). The intersection points indicate where the actual thickness is equal to the critical thickness.

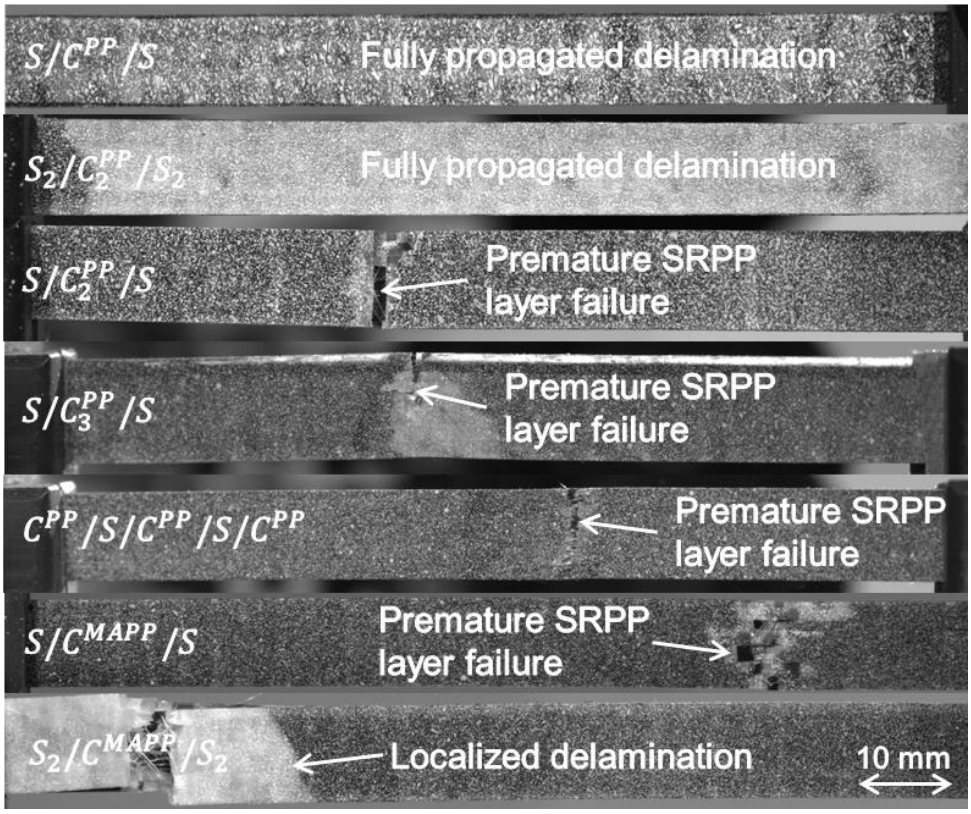


Fig. 9. Morphology of the samples at the moment of failure with the whitening region indicating delamination.

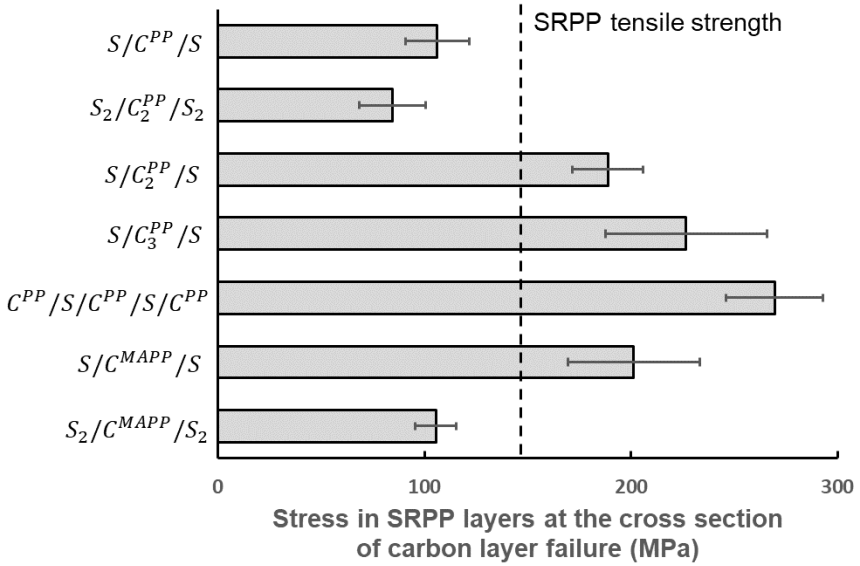


Fig. 10. Stress in SRPP layers at the cross-section of carbon layer failure in comparison to the strength of SRPP (at the moment when carbon layer fails).

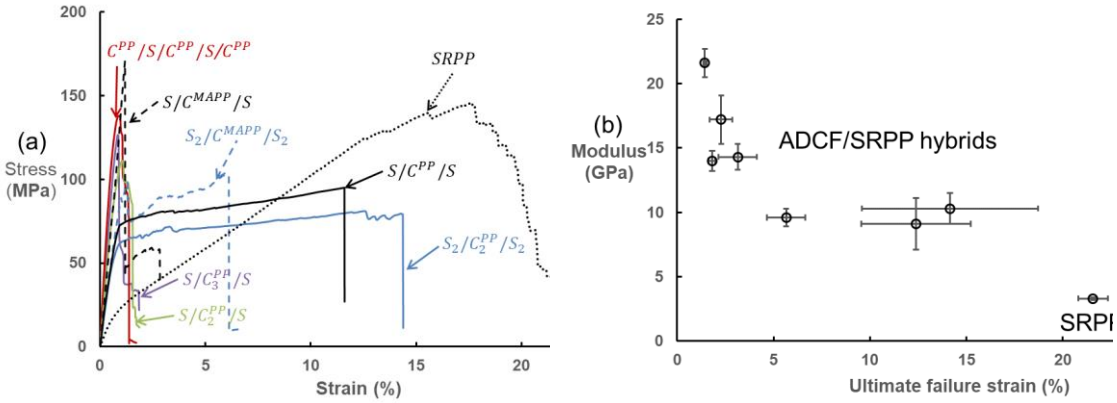


Fig. 11. (a) Representative stress-strain diagrams for all the hybrid layups including pure SRPP and (b) trade-off between modulus and ultimate failure strain.

Table 1. Engineering constants of the carbon fibers and the PP matrix [8, 22].

| | Tenax C124 | PP matrix |
|---|---|---|
| Longitudinal modulus (GPa) | 225 | 1.5 |
| Transverse modulus (GPa) | 15 | 1.5 |
| Longitudinal Poisson's ratio | 0.25 | 0.45 |
| In-plane shear modulus (GPa) | 20 | 0.52 |

Table 2. Composites specifications: thickness, fiber volume fraction and modulus of carbon layer.

| Hybrid layup | Overall thickness, $t_h$ (mm) | Overall carbon fiber volume fraction, $V_{f,h}$ (%) | Total carbon layer thickness, $t_{CFPP}$ (mm) | Carbon fiber volume fraction in carbon layer, $V_{f,CFPP}$ (%) | Modulus of carbon layer based on ROM (GPa) |
|---|---|---|---|---|---|
| $S/C^{PP}/S$ | 0.389 ± 0.017 | 6.5 ± 0.5 | 0.109 ± 0.014 | 23.2 ± 2.7 | 28.1 ± 3.1 |
| $S_2/C_2^{PP}/S_2$ | 0.754 ± 0.064 | 8.1 ± 1.0 | 0.194 ± 0.016 | 31.4 ± 2.8 | 26.0 ± 7.9 |
| $S/C_2^{PP}/S$ | 0.501± 0.015 | 10.0 ± 0.2 | 0.221 ± 0.004 | 22.7 ± 0.7 | 27.5 ± 2.0 |
| $S/C_3^{PP}/S$ | 0.543 ± 0.053 | 15.9 ± 0.6 | 0.264 ± 0.031 | 32.9 ± 3.3 | 32.2 ± 5.0 |
| $C^{PP}/S/C^{PP}/S/C^{PP}$ | 0.575 ± 0.027 | 15.9 ± 1.1 | 0.295 ± 0.005 | 30.9 ± 1.9 | 39.0 ± 1.9 |
| $S/C^{MAPP}/S$ | 0.382 ± 0.012 | 8.1 ± 0.4 | 0.104 ± 0.009 | 29.8 ± 2.6 | 43.9 ± 5.0 |
| $S_2/C^{MAPP}/S_2$ | 0.705 ± 0.020 | 4.9 ± 0.3 | 0.108 ± 0.005 | 30.5 ± 2.9 | 42.2 ± 5.2 |

Table 3. Tensile properties of SRPP and hybrid SCF/SRPP composites.

| Hybrid layup | Modulus (GPa) | Strength (MPa) | Ultimate failure strain (%) | Strain at carbon layer failure (%) | Stress at carbon layer failure (MPa) |
|---|---|---|---|---|---|
| SRPP | 3.3 ± 0.1 | 142.0 ± 4.0 | 21.57 ± 0.77 | - | - |
| $S/C^{PP}/S$ | 10.3 ± 1.2 | 105.0 ± 11.9 | 14.15 ± 4.56 | 0.94 ± 0.03 | 76.3 ± 8.5 |
| $S_2/C_2^{PP}/S_2$ | 9.1 ± 2.0 | 76.9 ± 7.4 | 12.39 ± 2.83 | 0.89 ± 0.04 | 62.7 ± 12.1 |
| $S/C_2^{PP}/S$ | 14.0 ± 0.8 | 105.5 ± 9.7 | 1.81 ± 0.18 | 1.00 ± 0.11 | 105.5 ± 9.7 |
| $S/C_3^{PP}/S$ | 17.2 ± 1.9 | 117.2 ± 23.6 | 2.28 ± 0.59 | 0.82 ± 0.05 | 117.2 ± 23.6 |
| $C^{PP}/S/C^{PP}/S/C^{PP}$ | 21.6 ± 1.1 | 131.2 ± 9.7 | 1.44 ± 0.07 | 0.87 ± 0.02 | 131.2 ± 9.7 |
| $S/C^{MAPP}/S$ | 14.3 ± 1.0 | 146.8 ± 23.7 | 3.14 ± 1.00 | 1.07 ± 0.16 | 146.8 ± 23.7 |
| $S_2/C^{MAPP}/S_2$ | 9.6 ± 0.7 | 92.8 ± 8.7 | 5.65 ± 1.00 | 1.29 ± 0.05 | 88.6 ± 8.4 |

Table 4. Failure modes of the hybrid composites.

| Failure mode | Edge-view schematics of the failure mode | Hybrid layups |
|---|---|---|
| Single carbon layer failure + premature SRPP layers failure | 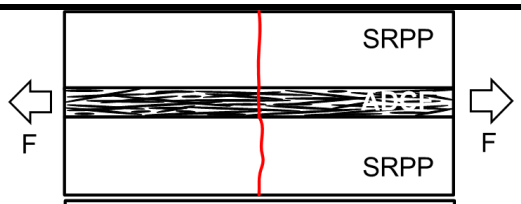 | $S/C_2^{PP}/S$, $S/C_3^{PP}/S$, $C^{PP}/S/C^{PP}/S/C^{PP}$, $S/C^{MAPP}/S$ |
| Carbon layer fragmentation + dispersed delamination | 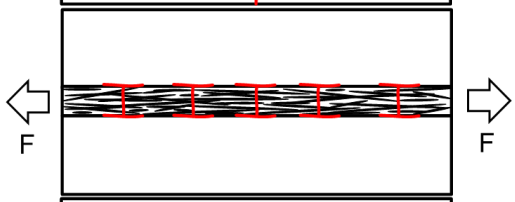 | $S/C^{PP}/S$, $S_2/C_2^{PP}/S_2$ |
| Single carbon layer failure + single delamination growth | 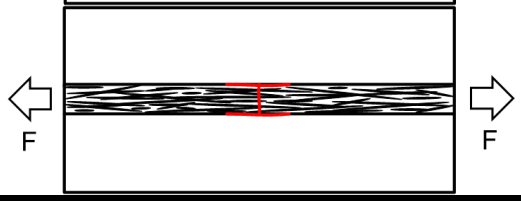 | $S_2/C^{MAPP}/S_2$ |